Cryo-EM structure of the human G-protein coupled receptor 1 (GPR1) – Gi protein complex bound to the chemerin C-terminal nonapeptide

Aijun Liu[1,4], Yezhou Liu[1,3,4], Geng Chen[1], Wenping Lyu[2], Junlin Wang[1], Fang Ye[1], Lizhe Zhu[2], Yang Du[1], Richard D. Ye[1,3,*]

[1]Kobilka Institute of Innovative Drug Discovery, and [2]Warshel Institute for Computational Biology, School of Medicine, The Chinese University of Hong Kong, Shenzhen, Guangdong, 518172, P.R. China; [3]Shenzhen Bay Laboratory, Shenzhen, Guangdong, 518055, P.R. China

[4]These authors contributed equally to this work.

[*]Corresponding author: Prof. Richard D. Ye (richardye@cuhk.edu.cn)

ABSTRACT

Chemerin is a chemoattractant and adipokine protein that acts on G protein-coupled receptors including chemokine-like receptor 1 (CMKLR1), G-protein coupled receptor 1 (GPR1) and C-C chemokine receptor-like 2 (CCRL2), mainly through its C-terminal peptide containing the sequence YFPGQFAFS (C-terminal nonapeptide or C9). Previous studies suggest that the three receptors respond to chemerin and C9 differently, with activation of the Gi signaling pathway through CMKLR1 but not GPR1 and CCRL2. Recently we reported a cryo-EM structure of human CMKLR1 in complex with Gi proteins and the C9 peptide. To identify structural differences among these receptors in ligand binding and Gi protein signaling, here we report a high-resolution cryo-EM structure of human GPR1-Gi complex bound to C9. Our structural and functional results show that GPR1 is able to respond to the C9 peptide with activation of the Gi signaling pathway and forms complex with a Gi protein. Similar to the CMKLR1-C9 structure, C9 adopts a C-terminus-in and S-shaped pose in the binding pocket. C9 is stabilized through hydrophobic interactions involving its Y1, F2, Q5, F6 and F8, and polar interactions between the P3, G4, Q5, F6, F8, S9 and residues lining the GPR1 binding pocket. An analysis of the GPR1-Gi protein interface found high similarities to the CMKLR1-Gi complex, and site-directed mutagenesis with functional verifications support GPR1 as a Gi-coupling receptors. These findings provide a structural basis of ligand recognition and Gi protein coupling by GPR1, and may help to understand the respective functions of the three chemerin receptors.

Keywords: GPCRs, chemerin, G proteins, cryo-EM

MAIN TEXT

Introduction

Chemerin is a small protein encoded by the *retinoic acid receptor responder 2* gene. Chemerin is mainly expressed in adipose tissue, liver, lung and skin (Bozaoglu et al., 2007; Goralski et al., 2007; Lehrke et al., 2009). The role of chemerin was initially identified as a chemoattractant of inflammatory cells following its discovery in psoriasis (Kennedy & Davenport, 2018a). Chemerin was subsequently found to act as an adipokine (Bozaoglu et al., 2007; Goralski et al., 2019; Goralski et al., 2007; Helfer & Wu, 2018). Secretion of chemerin requires removal of the N-terminal signaling peptides, resulting in pro-chemerin (amino acid 21-163) with a low biological activity. Further proteolytic removal of six amino acids from the C-terminus (158-163) leads to chemerin21-157 with full bioactivity (Wittamer et al., 2003). C-terminal synthetic fragments of human chemerin, including chemerin149-157 (C9), chemerin145-157 (C13) and chemerin138-157 (C20), show comparable biological activity to chemerin21-157 (Meder et al., 2003; Zabel, Allen, et al., 2005; Zabel, Silverio, et al., 2005).

To date, 3 chemerin receptors have been identified, namely chemokine-like receptor 1 (CMKLR1), G protein-coupled receptor 1 (GPR1) and C-C chemokine receptor-like 2 (CCRL2) (Barnea et al., 2008; Zabel et al., 2008). CMKLR1 responds to chemerin and the C9 peptide with activation of the G protein (Gi) pathway and the β-arrestin pathway. In contrast, CCRL2 binds chemerin but does not mediate its transmembrane signaling (Kennedy & Davenport, 2018a). The biological functions of GPR1 as a chemerin receptor remains unclear. GPR1 was originally identified as an orphan receptor (Marchese et al., 1994). It was subsequently found as a chemerin receptor but published studies of its pharmacological properties vary widely. Using a reporter assay (TANGO) for measurement of β-arrestin activation, Barnea *et al* found that GPR1 activation is biased towards the β-arrestin pathway when compared with CMKLR1 (Barnea et al., 2008). Another study showed that both CMKLR1 and GPR1 could activate the β-arrestin pathway but the amplitude of the CMKLR1-mediated signaling was larger (De Henau et al., 2016). In terms of G protein activation, published studies showed downstream activities of RhoA/ROCK, $G\alpha_{q/11}$ and $G\alpha_{i/o}$, but it was not clear which one is the dominant G protein for functional coupling

(Rourke et al., 2015). Other studies have shown that human GPR1 was involved in human immunodeficiency virus replication (Samson et al., 1998; Shimizu et al., 2009; Tokizawa et al., 2000), in glucose homeostasis, cardiovascular diseases, steroid hormone synthesis and reproductive biology (Caulfield et al., 2003; Ernst & Sinal, 2010; Karagiannis et al., 2013; Kennedy & Davenport, 2018a; Neves et al., 2018; Rourke et al., 2014), suggesting that the downstream signaling network of GPR1 may be diverse.

GPR1 and CMKLR1 share more than 80% of sequence homology, yet their respective functions elicited by chemerin may be different. CMKLR1 is often considered a balanced receptor mediating all biological functions of chemerin. In a recent study, we reported the cryo-EM structure of CMKLR1-Gi complex bound to the C9 peptide of chemerin (Wang et al., 2023) that illustrates a clearly defined binding pocket for the C-terminal peptide of chemerin as well as an interface for Gi protein interaction. For GPR1, studies support the ligand-induced β-arrestin recruitment, yet current findings on the activation of G protein signaling by GPR1 are inconsistent and controversial (De Henau et al., 2016; Kennedy & Davenport, 2018a). Given the discrepancies among current understandings of GPR1 downstream signaling pathways, it is important to understand how chemerin binds to GPR1 and whether the binding event can be translated into G protein activation. To this end, we have determined the cryo-EM structure of GPR1 bound to C9, in complex with heterotrimeric Gi proteins. Our results demonstrated the structural basis for GPR1-dependent Gi protein activation.

Methods

Expression vector design

Human GPR1 was cloned into a pFastBac vector (Invitrogen, Carlsbad, CA, USA) for protein expression towards purification. Specifically, to improve the expression yield as well as the protein stability, the coding sequence of human GPR1 was fused with an N-terminal HA signal peptide followed by a FLAG tag, a human rhinovirus 14 3C (HRV-3C) protease cleavage site (LEVLFQGP) and the thermostabilized apocytochrome b(562)RIL (BRIL) fusion protein (Chun et al., 2012). Human dominant negative Gαi1 (DNGαi1), generated by site-directed mutagenesis of G203A and A326S in Gαi1, was cloned into a pFastBac vector. N-terminal 6×His-tagged Gβ1 and Gγ2 were cloned into a pFastBac-Dual vector. scFv16 was fused with a N-terminal GP67 signal peptide and a C-terminal 8× His tag, and the coding sequence was then cloned into a pFastBac vector.

For functional assays, the full-length human GPR1 cDNA were cloned into pcDNA3.1(+) vector (Invitrogen) with an N-terminal FLAG tag. Point mutations were introduced using homologous recombination. Two fragments of GPR1 separated at mutated positions were amplified using PCR and then assembled into pre-cut pcDNA3.1(+) vectors using the ClonExpress Ultra One Step Cloning Kit (Vazyme Biotech; C115). Plasmids with GPR1 mutations were confirmed by DNA sequencing (GENEWIZ).

Expression and purification of the GPR1-Gi complexes

The baculoviruses of GPR1, DNGαi1, Gβ1 and Gγ2 were generated and amplified using the Bac-to-Bac baculovirus expression system vector. The *Sf*9 cells were cultured in SIM SF Expression Medium (Sino Biological). When the cell density reached 3.5×10^6 cells/mL (in total 2 liters), the three types of baculoviruses (GPR1, DNGαi1, Gβ1γ2) were co-expressed in *Sf*9 cells at a ratio of 1:4:2 (total volume of baculoviruses: 26 mL). After infection for 60 hrs, the cells were collected by centrifugation at 2,000 × g for 15 mins and kept frozen at −80 °C for complex purification.

For the purification of C9 bound GPR1-Gi protein complexes, cell pellets from the 2L culture were resuspended in 150 mL lysis buffer (10 mM Tris pH 7.5, 1 mM EDTA, 2.5 μg/mL leupeptin and 160 μg/mL benzamidine, 4 μM C9 peptide and 1 mg/mL iodoacetamde) for 30 mins at room temperature. The lysate was centrifuged for 15 mins at 18,000 × g, and pellet was homogenized in 150 mL solubilization buffer (20 mM HEPES pH 7.5, 100 mM NaCl, 10% glycerol, 1% dodecylmaltoside (DDM), 0.1% cholesteryl hemisuccinate (CHS), 2.5 μg/mL leupeptin and 160 μg/mL benzamidine, 4 μM C9 peptide, 1 mg/mL iodoacetamde, 2 mg scFv16, 25 mU/mL apyrase) using a dounce-homogenizer. The sample was stirred for 2 hrs at 4°C and then centrifuged for 30 mins at 18,000 × g to remove the insoluble debris. The solubilized supernatant fraction was incubated with 2 mL anti-FLAG affinity resin (GenScript Biotech, Piscataway, NJ) and stirred at 4˚C for 2 hrs. Then, the resin was manually loaded onto a gravity-flow column and extensively washed with the FLAG wash buffer (W1: 20 mM HEPES pH 7.5, 0.1% DDM, 0.01% CHS, 100 mM NaCl, 2 mM $CaCl_2$, 4 μM C9 peptide. W2: 20 mM HEPES pH 7.5, 0.2% lauryl maltose neopentyl glycol (LMNG), 0.02% CHS, 100 mM NaCl, 2 mM $CaCl_2$, 4 μM C9 peptide) by mixing W1

and W2 buffer in the following ratios: 5 mL:5 mL, 2 mL:8 mL, 1 mL:9 mL, 0.5 mL:9.5 mL, 0 mL:10 mL, respectively. The GPR1-Gi complexes attached to the resin were further eluted with 10 mL elution buffer (20 mM HEPES pH 7.5, 0.01% LMNG, 0.002% CHS, 100 mM NaCl, 4 μM C9 peptide, 5 mM EDTA, 0.2 mg/ml FLAG peptide). Eluted protein complexes were concentrated to 400 μL in an Amicon® Ultra-15 Centrifugal Filter Unit (Millipore, Burlington, MA) and further subjected to a size exclusion chromatography through a Superdex 200 Increase 10/300 column (GE Healthcare Life Sciences, Sweden) equipped in an AKTA FPLC system with running buffer (20 mM HEPES pH 7.5, 0.01% LMNG, 0.002% CHS, 100 mM NaCl, 4 μM C9 peptide). Eluted fractions containing GPR1-Gi complexes were re-pooled and concentrated as described above before being flash frozen in liquid nitrogen and stored at −80 ˚C.

Expression and purification of scFv16

The antibody fragment scFv16 was expressed as a secretory protein and purified as previously described (2). Briefly, *Trichoplusia ni* Hi5 insect cells were cultured to reach a density of 3.5×10^6 cells/mL. Cells were then infected with scFv16 baculovirus at a ratio of 1:50. After 60 hrs of culture, the supernatant was collected and loaded onto a Ni-NTA resin column. The column was washed with 20 mM HEPES (pH 7.5), 500mM NaCl, and 20 mM imidazole, and then subjected to elution by 20 mM HEPES (pH 7.5), 100 mM NaCl, and 250 mM imidazole. The eluted proteins were concentrated and subjected to size-exclusion chromatography using a Superdex 200 Increase 10/300 column (GE Healthcare). Finally, the purified scFv16 protein with a monomeric peak was concentrated and flash frozen in liquid nitrogen and stored at −80 ˚C for further use.

Cryo-EM sample preparation and data collection

For cryo-EM sample preparation of the C9-GPR1-Gi-scFv16 complex, amorphous alloy film (CryoMatrix nickel titanium alloy film, R1.2/1.3, Zhenjiang Lehua Electronic Technology Co., Ltd.) was glow discharged in a Tergeo-EM plasma cleaner. 3 μL purified complex sample was loaded on the grid and blotted for 3 s with a blotting force of 0, and then flash-frozen in liquid ethane cooled by liquid nitrogen using Vitrobot Mark IV (Thermo Fisher Scientific, Waltham, MA). For data collection, cryo-EM data were collected at the Kobilka Cryo-EM Center of The Chinese University of Hong Kong, Shenzhen, on a 300 kV Titan Krios Gi3 microscope (Thermo Fisher Scientific). The raw movies were then recorded using a Gatan K3 BioQuantum Camera at the magnification of 105,000, with the pixel size of 0.83 Å. A GIF Quantum energy filter was applied to exclude inelastically scattered electrons (Gatan, USA) using a slit width of 20 eV. The movie stacks were acquired with a total exposure time of 2.5 s fragmented into 50 frames (0.05 s/frame). The defocus range were from −1.2 to −2.0 μm. The semi-automatic data acquisition was performed using SerialEM. A total of 3,609 image stacks were collected in 60 hrs.

Image processing and model building

Data processing was performed with cryoSPARC 3.3.1 (Structura Biotechnology Inc., Toronto, Canada). Patch motion correction and patch CTF estimation were firstly applied to the image stacks. 2,280,697 particles were auto-picked. 2D classification was performed, resulting in 732,629 particles selected for *ab initio* reconstruction. After 3 rounds heterogeneous refinements, a final set of 339,859

particles were exported to non-uniform refinement and local refinement, yielding a map with global resolution of 2.90 Å.

The predicted structure GPR1 on AlphaFold database was used to build the initial model of the receptor. The coordinates of Gi1 and scFv16 from GPR88 (PDB ID: 7WXZ) were applied as templates. All models were docked into the EM density map using UCSF Chimera version 1.12, followed by iterative manual building in Coot-0.9.2 and refinement in Phenix-1.18.2. The statistics of the final model were further validated by Phenix-1.18.2. Structure figures were generated by Chimera or PyMOL (Schrödinger, Inc., New York, NY). The statistics of data-collection and structure-refinement were shown in Supplementary Table 1.

Molecular modeling and molecular dynamic simulation

Protonation state of the GPR1 was assigned by the web server H++ (Anandakrishnan et al., 2012) assuming pH 7.4, and charmm36m (Anandakrishnan et al., 2012) force field was employed in all simulations. After energy minimization, membrane relaxation, and equilibrium simulation (Huang et al., 2017), ten independent 1-μs long production MD simulations were carried out for C9/GPR1 complex. 50,000 conformations were collected in total from the assemble of trajectories. Hydrogen bonds were identified based on cutoffs for the Donor-H⋯Acceptor distance and angle. The criterion employed was angle > 120° and H⋯Acceptor distance < 2.5 Å in at least 10% of the trajectory.

G protein dissociation assay

G protein activation was tested by a NanoBiT-based G protein dissociation assay (Inoue et al., 2019). HEK293T cells were plated in a 24-well plate 24 hrs before transfection. Lipofectamine™ 3000 (Invitrogen, L3000001) transfection was performed with a mixture of 92 ng pcDNA3.1 vector encoding human GPR1 (WT/mutants) or WT human CMKLR1 for comparison, 46 ng pcDNA3.1 vector encoding Gαi1-LgBiT, 230 ng pcDNA3.1 vector encoding Gβ1 and 230 ng pcDNA3.1 vector encoding SmBiT-Gγ2 (per well in a 24-well plate), respectively. After 24 hrs incubation, the transfected cells were collected and resuspended in HBSS containing 20 mM HEPES. The cell suspension was loaded onto a 384-well culture white plate (PerkinElmer Life Sciences, Waltham, MA) at a volume of 20 μL and loaded with 5 μL of 50 μM coelenterazine H (Yeasen Biotech, Shanghai, China). After 2 hrs incubation at room temperature, the baseline was measured using a Envision 2105 multimode plate reader (PerkinElmer, Waltham, MA, USA). Then, C9 peptides (ChinaPeptides, Shanghai, China) were added to the cells to different concentration. The ligand-induced luminescence signals were measured 15 mins after ligand addition and divided by the initial baseline readouts. The fold changes of signals were further normalized to PBS-treated signal and the values (EC_{50}) were expressed as a function of different concentrations of C9 peptide ligand based on three independent experiments, each with triplicate measurements.

cAMP assay

Wild-type human GPR1 and its mutants, or wild-type human CMKLR1 for comparison, were transiently expressed in HeLa cells 24 hrs prior to collection. The cells were resuspended in HBSS buffer plus 5 mM HEPES, 0.1% BSA (w/v) and 0.5 mM 3-isobutyl-1-methylxanthine and loaded onto 384-well plates. Different concentrations of C9 peptide were prepared with 2.5 μM forskolin in the

abovementioned buffer. The cells were stimulated by the ligands and 2.5 μM forskolin for 30 mins in a cell incubator. Intracellular cAMP levels were measured with the LANCE Ultra cAMP kit (PerkinElmer, TRF0263) following the manufacturer's instructions. In the measurements, signals of time resolved-fluorescence resonance energy transfer (TR-FRET) were detected by a EnVision 2105 multimode plate reader (PerkinElmer). Intracellular cAMP levels were calculated according to the TR-FRET signals of the samples and cAMP standards.

β-arrestin recruitment assay

For NanoBiT-based β-arrestin recruitment assay, HEK293T cells were seeded in a 24-well plate 24 hrs before transfection. Cells are co-transfected with GPR1-WT-smBiT or CMKLR1-WT-smBiT (400 ng/well) and LgBiT-β-Arr1 or LgBiT-β-Arr2 (200 ng/well) by Lipofectamine™ 3000 (Invitrogen) for 24 hrs. Cells were collected and resuspended in HBSS buffer containing 20 mM HEPES, and then 20 μL of cell suspension was loaded onto a 384-well white plate at a concentration of $2x10^4$ cells/well. Test samples were further loaded with coelenterazine H to a final concentration of 10 μM. After 25 mins incubation at 37 °C, the samples were measured for baseline luminescence using Envision 2105 multimode plate reader (PerkinElmer). Different concentrations of C9 peptide were added to the wells and the luminescence signals were detected for 30 mins. The signal readouts were further normalized to PBS-treated signal and the values (EC_{50}) were expressed as a function of different concentrations of C9 peptide ligand based on three independent experiments, each with triplicate measurements.

IP one accumulation assay

Wild-type GPR1 and its mutants, and wild-type human CMKLR1 for comparison, were transiently expressed in HEK293T cells for 24 hrs. IP one accumulation was tested using IP-One Gq HTRF kit (Cisbio). The cells were resuspended in the stimulation buffer (Cisbio) and incubated with different concentrations of C9 peptide diluted in the stimulation buffer for 30 mins at 37 °C. The accumulation of IP one was further determined following the manufacturer's protocols. Fluorescence intensities were measured on a Envision 2105 multimode plate reader (PerkinElmer). Intracellular IP one levels were calculated according to the fluorescence signals of the samples and IP one standards.

GPR1 expression level determination by flow cytometry

HEK293T cells were transfected with FALG-tagged WT or mutant GPR1 expression plasmids for 24 hrs at 37°C. Then the cells were harvested and washed in HBSS containing 5% BSA for three times on ice. The cells were then incubated with a FITC-labeled anti-FLAG antibody (M2; Sigma, Cat #F4049; 1:50 diluted by HBSS buffer) for 30 mins on ice and washed with HBSS. The FITC fluorescence signals demonstrating the antibody-receptor complex on the cell surface were quantified by flow cytometry (CytoFLEX, Beckman Coulter, Brea, CA). Relative expression levels of GPR1 mutants were represented according to the fluorescence signals.

Statistical analysis

The data were analyzed with Prism 9.5.0 (GraphPad, San Diego, CA). For dose-response analysis, the curves were plotted with the log[agonist] vs. response equation (three parameters) in the software. For cAMP, IP one, and G-protein dissociation assays, data points were presented as the percentages (mean ± SEM)

of the maximal response level for each sample, from at least three independent experiments, as indicated in figure legends. For the β-arrestin recruitment assay, data were presented as raw chemiluminescence signals (mean ± SEM) from at least three independent experiments. The EC_{50} values were obtained from the dose-response curves. For cell surface expression, data points were presented as the percentages (mean ± SEM) of the flow cytometry fluorescence signals of WT GPR1. For statistical comparisons, Analysis of Variance (ANOVA) was performed using the one-way method. A *p* value of 0.05 or lower is considered statistically significant.

329 **Results**

330

331 **GPR1 can activate Gi protein responses.**

332 It has been long controversial about the downstream signaling events elicited by the
333 activation of GPR1. We hence compared GPR1 and CMKLR1 by performing G
334 protein dissociation assay, cAMP inhibition assay targeting the Gαi responses, IP
335 one accumulation assay targeting Gβγ downstream events and β-arrestin
336 recruitment assays. Although to a significantly less extent in comparison with
337 CMKLR1, GPR1 can elicit cAMP inhibition (Fig. 1A). In NanoBiT G protein
338 dissociation assay, C9 activates GPR1 and CMKLR1 with a similar EC_{50}, although
339 the efficacy is lower for GPR1 (Fig. 1B). IP one accumulation as a downstream
340 signaling event of Gβγ proteins observed a lower EC_{50} for GPR1 with a similar
341 amplitude (Fig. 1C). These results identify that GPR1 can activate a weak G protein
342 response. We further extended our functional test to β-arrestin recruitment. Both
343 CMKLR1 and GPR1 showed a preference in recruiting β-arrestin 1 (Fig. 1D). GPR1
344 experienced a significant lower efficacy of β-arrestin responses, with nearly no
345 recruitment of β-arrestin 2. This finding corresponds to previous discoveries by other
346 groups with respect to downstream signaling events of chemerin receptors (Barnea
347 et al., 2008; De Henau et al., 2016; Degroot et al., 2022; Fischer et al., 2021;
348 Kennedy & Davenport, 2018b; Rourke et al., 2015; Wittamer et al., 2003).

349

350 **Cryo-EM structure of the GPR1-Gi complex.**

351 The GPR1-Gi-scFv16 protein complex bound to the chemerin nonapeptide C9 (149-
352 YFPGQFAFS-157) was prepared and the structure was determined by cryo-EM to
353 an overall resolution of 2.90 Å (Fig. 2A and B, Fig. S1 and S2). The antibody
354 fragment scFv16 was used for stabilization of the C9-GPR1-Gi complex (Maeda et
355 al., 2018). Heterotrimeric Gi proteins, including Gαi, Gβ and Gγ, associate with the
356 receptor to form the complex. The ligand-binding pocket of GPR1 was surrounded by
357 transmembrane (TM) helices 2, 3, 4, 6, 7 and the first, second and third extracellular
358 loops (ECL1, ECL2 and ECL3) (Fig. 2A). The C9 peptide assumes a posture with its
359 C terminus inserted to the binding pocket (Fig. 2 B-D), and the peptide ligand takes
360 an “S”-shape in the binding pocket, providing interactions between the ligand and the
361 receptor residues. Specifically in this structural model (Fig. 2 C-E), the N-terminal Y1
362 and F2 of the C9 peptide show hydrophobic interactions with $L186^{ECL2}$, $H273^{ECL3}$,

363 Y188^{ECL2} and I272$^{6.61}$[superscripts indicate the Ballesteros-Weinstein numbering
364 scheme for GPCRs (Ballesteros & Weinstein, 1995)]. P3 in the peptide backbone
365 formed polar interactions with N189^{ECL2} and G4 has polar interactions formed
366 between its backbone amide group and E269$^{6.58}$. Q5 with its backbone carbonyl
367 oxygen formed polar interaction with Y96$^{2.63}$. The aromatic ring of F6 showed
368 nonpolar interactions with F101^{ECL1} and Q283$^{7.32}$, and the backbone carbonyl oxygen
369 has polar interactions with Y93$^{2.60}$. F8 with its aromatic ring showed extensive
370 hydrophobic interactions with residues P287$^{7.36}$, I286$^{7.35}$, C187^{ECL2}, T290$^{7.39}$, A117$^{3.32}$
371 and M121$^{3.36}$ to stabilize the peptide ligand in the binding pocket. S9 at the C-
372 terminal end of the C9 peptide experienced polar interactions extensively with
373 S114$^{3.29}$, Q118$^{3.33}$ and R176$^{4.64}$ with its carbonyl and side chain oxygens. To note,
374 Q$^{3.33}$ is an amino acid residue conserved in some chemoattractant GPCRs including
375 FPR1 and FPR2 (Chen et al., 2022; Chen et al., 2020; Zhu et al., 2022; Zhuang et
376 al., 2020; Zhuang et al., 2022). The aromatic ring of F8 inserts deep into the binding
377 pocket, pointing just above the “toggle switch” W259$^{6.48}$ of GPR1 for G protein
378 activation (Weis & Kobilka, 2018). By comparing between the structures of GPR1-C9
379 and CMKLR1-C9, the C9 ligand bound to GPR1 was measured to have an average
380 of 1.2 Å upward shift, and the residues in contact with the ligand were closer to the
381 extracellular loop of GPR1 (Fig. S3). These binding site findings suggest that despite
382 the ligand C9 peptide takes a similar pose in the binding pocket, the binding of C9 to
383 GPR1 is shallower than that in the case of CMKLR1.
384
385 **Functional analysis of the GPR1-C9 interaction.**
386 Following the structural model of GPR1, site-directed mutagenesis of the receptor
387 was conducted to confirm the interactions between the ligand C9 peptide and the
388 receptor binding pocket. Alanine substitutions of the key residues in the binding
389 pocket of GPR1 were followed by functional assays of the mutants in cAMP inhibition
390 assay and G protein dissociation assay respectively to measure the activation of
391 GPR1 by the C9 peptide (Fig. 3). The results from these two assays were consistent.
392 The alanine substitution of residues forming polar interactions with the C9 peptide,
393 including N189^{ECL2}, E269$^{6.58}$, Y96$^{2.63}$, Y93$^{2.60}$, S114$^{3.29}$, Q118$^{3.33}$ and R176$^{4.64}$,
394 resulted in a remarkable decrease in the potency of the ligand (Fig. 3, A-C and E-G).
395 Of note, Y96$^{2.63}$A and E269$^{6.58}$A mutants completely diminished the response. For
396 the extensive polar interactions between S9 of the C9 peptide and the receptor, we

397 observed that single point mutations of S114$^{3.29}$, Q118$^{3.33}$ or R176$^{4.64}$ did not
398 completely eliminate the response. This could be due to the flexibility at S9 of the
399 ligand where multiple hydrogen bonds may form alternatively between the carbonyl
400 and side chain oxygens of S9 and S114$^{3.29}$, Q118$^{3.33}$ or R176$^{4.64}$ of GPR1 (Fig. 3, A,
401 B, E and F). Indeed, by introducing a triple mutation at S114-Q118-R176, the cAMP
402 inhibition and G protein dissociation responses were completely abolished (Fig. 3, D
403 and H). These results altogether supported the role of the substituted amino acid
404 residues in hydrogen bond formation with P3, G4, Q5, F6 and S9 of the C9 peptide.
405
406 In addition to polar interactions, hydrophobic interactions also play an important role
407 in C9 interaction with GPR1. Mutations of some nonpolar residues in the binding
408 pocket of GPR1, including L186^{ECL2}, Y188^{ECL2}, Q283$^{7.32}$ and T290$^{7.39}$, reduced the
409 potency of cAMP inhibition and G protein responses (Fig. 3, C, D, G and H). And a
410 greater reduction in functional efficacy was observed for T290$^{7.39}$A, as both cAMP
411 inhibition and G protein dissociation were almost completely lost. Taken together,
412 site-directed mutagenesis and corresponding functional assays results are in line
413 with the cryo-EM structural model of C9-bound GPR1.
414
415 **Thermodynamic stability of GPR1-C9 interface**
416 Full-atom molecular dynamics (MD) simulations were performed for GPR1-C9
417 complex at room temperature (10 replicas of 1-μs-long simulation). In these MD
418 trajectories, the complex captured by Cryo-EM were overall stable under
419 thermodynamic perturbation (Fig. S5), and the binding pose of the C9 peptide were
420 well kept through the assemble of 1-μs trajectories (Fig. 4). Except the hydrophobic
421 residue F2, we observed that 8 residues out of the 9 residues on C9 peptide form
422 hydrogen-bonds (H-bonds) with GPR1 (Fig. 4). The residues close to the C-terminal
423 of the C9 peptide formed several H-bonds with Y96$^{2.63}$, N189^{ECL2}, R176$^{4.64}$, S114$^{3.29}$,
424 Y262$^{6.51}$, and K210$^{5.42}$. Among these, N189^{ECL2} and Y96$^{2.63}$ also formed H-bonds
425 with P3 and Q5 on the C9 peptide. The N-terminal of C9 peptide was more likely to
426 interact with negatively charged E269$^{6.58}$. The latter also interacted with G4, while
427 the G4 formed a stable H-bond with R176$^{4.64}$ (Fig. 4B). These interactions resulted in
428 a complex network between C9 and the receptor, which rationalized the
429 thermodynamic stability of the C9 peptide in the binding pocket of GPR1.
430

431 By comparing the EC_{50} of cAMP assays, we found that the $N189^{ECL2}$ and $Y96^{2.63}$,
432 which have the top 2 occupancy on single H-bond (Fig. 4A), are the most functionally
433 important ($-logEC_{50} = 0$, i.e., no effect on cAMP inhibition). Another functional
434 important residue is $E269^{6.58}$ ($-logEC_{50} = 0$), which has less single H-bond
435 occupancy (<0.6, Fig. 4A), but with the highest overall H-bond occupancy
436 considering all associated H-bonds (>1.5). Therefore, we propose that the functional
437 effects of the C9 peptide is highly related to the polar interactions with GPR1.
438
439 **Activation mechanism of GPR1-Gi complex.**
440 To investigate the conformational changes associated with the activation of GPR1,
441 we compared the structure of active GPR1 and an antagonist-bound inactive C5aR
442 (C5aR-PMX53, PDB ID: 6C1R) as the most homologous GPCR to GPR1, or a C9-
443 bound active CMKLR1 (CMKLR1-C9, PDB ID: 7YKD), respectively (Fig. 5). From the
444 comparison between the active and inactive forms of receptors, an outward
445 movement of TM5 and TM6, and an inward movement of TM7 were observed (Fig.
446 5A). Specifically, for the $D^{3.49}$-$R^{3.50}$-$Y^{3.51}$ motif conserved for G protein activation
447 among Class A GPCRs, GPR1 presents the motif as D134-H135-Y136 and C5aR
448 presents it as DRF. Both receptors showed no interaction between $H^{3.50}$/$R^{3.50}$ and
449 $Y^{5.58}$ (Fig. 5B). The highly conserved residue $W259^{6.48}$ as a “toggle switch” of G
450 protein activation showed an anti-clockwise rotation in GPR1-C9 structure (Fig. 5C),
451 which marks the conformational rearrangement of such a toggle switch upon GPCR
452 activation (Weis & Kobilka, 2018; Zhou et al., 2019). For the $P^{5.50}$-I/$V^{3.40}$-$F^{6.44}$ motif,
453 rotamer conformational changes was displayed in the GPR1-C9 structure in
454 compare with the inactive C5aR structure (Fig. 5D). To further identify the structural
455 basis of different signaling responses of GPR1 and CMKLR1 upon C9 peptide
456 stimulation, we compared the active structures of the two receptors. An outward
457 movement of TM5, TM7 and an inward movement of TM6 was demonstrated (Fig.
458 5E). As for the DRY motif, CMKLR1 presents a DRC in position and $R^{3.50}$ formed a
459 polar interaction with the $Y^{5.58}$ residue (Fig. 5F). $H135^{3.50}$ in GPR1, however, pointed
460 to the cytosolic part with no observable polar interaction with adjacent receptor
461 residues. For the “toggle switch”, $W259^{6.48}$ in GPR1 shifted slightly upwards (Fig.
462 5G). Not much difference in the orientation of the $P218^{5.50}$-$V125^{3.40}$-$F255^{6.44}$ motif
463 was observed (Fig. 5H). Overall, by analyzing the geometry of important motifs for

464 receptor activation, the structure of GPR1 supports GPCR activation and also
465 explains a lower amplitude of downstream signaling responses.
466
467 Next, the interaction between an activated GPR1 and the Gi class of heterotrimeric
468 G proteins was examined. In this study, we adopted DNGαi1, a dominant negative
469 form of human Gαi1 which has mutations of G203A and A326S, for the decrease
470 affinity for nucleotide binding and increased stability of heterotrimeric G protein
471 complex (Lee et al., 1992; Posner et al., 1998). In the structure, the α5 helix of Gαi
472 inserted into the intracellular loops of GPR1, forming hydrophobic interactions with
473 F76$^{2.43}$, L151$^{4.39}$, V251$^{6.40}$, Y226$^{5.58}$, T247$^{6.36}$, K310$^{8.49}$ (Fig. 6A). Of note, some polar
474 interactions were expected between α5 helix G352 and GPR1 H135$^{3.50}$, α5 helix
475 N347 and GPR1 H138$^{3.53}$, αN helix R32 and GPR1 H146^{ICL2} (Fig. 6A). Additionally,
476 we also observed a hydrogen bond between GPR1 helix 8 and D312 of the Gβ
477 subunit (Fig. 6B).
478
479 The interaction between the heterotrimeric Gi protein and the receptor was
480 compared among other Gi-coupled GPCRs, including active CMKLR1 and CCR5
481 (PDB ID: 7F1R), inactive C5aR and CXCR4 (PDB ID: 3ODU) (Fig. 6 C-E). The
482 orientation of TM6 and TM7 marks the greatest difference between active and
483 inactive receptors (Fig. 6 C and D). For active receptors GPR1, CMKLR1 and CCR5,
484 TM6 displayed an outward tilt allowing the space for interface between the receptor
485 and C-terminal α5 helix of Gαi (Fig. 6C). Helix8 of the active receptors showed a
486 movement to the intracellular compartment for the engagement of Gβ subunit (Fig.
487 6C). An inward movement of TM7 was also observed for GPR1 and other active
488 receptors compared with the inactive representatives (Fig. 6D). Despite we did not
489 observe much polar interaction between GPR1 and the αN helix of Gαi as the case
490 in CMKLR1 (Wang et al., 2023), the αN helix of Gαi moved upwards for a closer
491 proximity with the receptor helix8 (Fig. 6E). These features contribute to the
492 activation of G protein by GPR1.
493
494 We further verified the proposed mechanisms of G protein activation by introducing
495 point mutations to the key residues. By substituting H135$^{3.50}$ into the canonical
496 arginine, the efficacy of cAMP inhibition increased with a decrease in the potency
497 (Fig. 7A). And the corresponding curve for G protein dissociation was similar with

498 that of the wild type GPR1 (Fig. 7B). Point mutations of P218$^{5.50}$-V125$^{3.40}$-F255$^{6.44}$
499 into alanine greatly reduced the cAMP response as well as the G protein dissociation
500 event (Fig. 7). The “toggle switch” W259$^{6.48}$ when substituted by alanine
501 demonstrated a complete loss in cAMP inhibition, yet the G protein dissociation has
502 been recovered with a decreased efficacy and potency (Fig. 7 C and F). For the
503 interaction interface between the receptor and Gαi, alanine substitution at H135$^{3.50}$,
504 H138$^{3.53}$ and H146^{ICL2} completely diminished G protein responses (Fig. 7 A-B and D-
505 E). All these function assays verified the importance of aforementioned key residues
506 in activating G protein responses.
507
508
509

Discussion

Chemerin is the natural ligand of CMKLR1, GPR1 and CCRL2. With a pronounced sequence similarity among these chemerin receptor, C-terminal nonapeptide C9 bearing the YFPGQFAFS sequence is responsible for GPR1 receptor activation and downstream signaling (De Henau et al., 2016; Fischer et al., 2021; Kennedy & Davenport, 2018b; Rourke et al., 2015; Schulz et al., 2022). However, despite two decades of effort since the original characterization of chemerin receptors, the structural basis for the respective functions and signaling pathways of the three chemerin receptors remain unclear. Although several studies implied a possible Gi coupling by GPR1, some other studies demonstrated an absence of G protein signaling event, thereby distinguishing GPR1 from CMKLR1 with full signaling capability. In this study, we report a cryo-EM structure of human GPR1-C9-Gi protein complex, providing structural evidence that GPR1 is able to couple to the Gi proteins. Examination into the structure and molecular dynamics of the ligand binding pocket revealed a shallower binding of C9 to GPR1 than CMKLR1. The analysis of the receptor-Gi protein interface found some polar interactions between the receptor and G protein heterodimer complex. Of note, the highly G protein-binding motif, $D^{3.49}$-$R^{3.50}$-$Y^{3.51}$, found in many Class A GPCRs, is replaced by DHY in GPR1. Notably, histamine substitution in this motif did not diminish G protein binding, and a polar interaction between $H135^{3.50}$ and α5 helix of Gi was even observed. Likewise, replacing the histamine residue with the original arginine residue did not significantly alter Gi protein coupling and downstream signaling. Altogether, our findings support GPR1 coupling to the Gi proteins.

It has been widely accepted that the GPR1 is generally weaker than its structural analog CMKLR1 in terms of the magnitude of its ligand binding and downstream signaling responses (De Henau et al., 2016; Degroot et al., 2022; Kennedy & Davenport, 2018a; Kennedy et al., 2016; Rourke et al., 2015; Rourke et al., 2014). Our structural and functional findings are consistent with those previous findings. By mapping into the structural details of the binding pocket, a shallower pocket for ligand insertion was observed in comparison to the one in CMKLR1 (Fig. S3). There are fewer C9 contact sites in the GPR1 binding pocket than in CMKLR1, thus affecting the extent of conformational changes necessary for full activation of the

receptor. Interestingly, the molecular dynamics trajectories of receptor-ligand interaction shows that the first 3 hydrogen bond-forming residues in the receptor fall into the same side of the ligand binding pocket (TM2, 3, 4), whereas the rest of these residues fall in the other side of the binding pocket, forming a major sub-pocket and a minor sub-pocket. Moreover, the majority of receptor residues with hydrophobic interactions are clustered around TM2 and TM7 (Fig. S5). This observation is similar to the division of major and minor sub-pockets in chemokine receptors, where the TM3-7 of chemokine receptors build the major sub-pocket and TM1-3 and TM7 identify the minor sub-pocket for chemokine binding (Kleist et al., 2016; Surgand et al., 2006). This feature of the ligand binding pocket may further our understanding of the similarities and differences between chemerin receptors and chemokine receptors.

While the structural information of GPR1 expands our knowledge in chemerin receptor biology, several unknowns still remain for further investigation. Given the high similarities between GPR1 and CMKLR1, they may share a variety of agonists and antagonists. Currently the only natural ligand of GPR1 and CMKLR1 is chemerin, and the wide distribution of GPR1 and CMKLR1 among immune cells, adipose tissues and central nervous system suggests the presence of other possible endogenous ligands (Herova et al., 2015; Marchese et al., 1994; Tokizawa et al., 2000; Wittamer et al., 2003; Wittamer et al., 2004). Indeed, a previous report unraveled a novel ligand of GPR1, FAM19A1, which is highly expressed in adult hippocampus and has neural modulatory effect (Zheng et al., 2018). However, there is still a lack of structural information about FAM19A1 interaction with GPR1, and the reported study was based primarily on animal experiments without a biochemical mechanism for receptor activation. Taken together, the cryo-EM structure of C9-bound GPR1-Gi complex structure provides valuable information for identification of signaling properties of chemerin receptors. The activation of GPR1 incorporates the coupling of Gi protein and its downstream signaling events, despite a less robust G protein response when compared with CMKLR1. These findings support a role for GPR1 in Gi protein activation, and point future research directions including the expression profile of these chemerin receptors in different tissues and organs, cross-desensitization of these receptors, and possible biased signaling through these receptors when more ligands become available.

578

579 **Acknowledgments**

580 This work was supported in part by grants from the Science, Technology and
581 Innovation Commission of Shenzhen Municipality GXWD20201231105722002-
582 20200831175432002 (R.D.Y., Y.D. and L.Z.), JCYJ20200109150019113 (Y.D.,
583 G.C.), JCYJ20200109150003938 (L.Z.), RCYX20200714114645019 (L.Z.) and
584 RCBS20221008093330067 (A.L.). This work was also supported by National Natural
585 Science Foundation of China 31971179 (L.Z.) and 32070950 (R.D.Y.), the
586 Fellowship of China Postdoctoral Science Foundation 2022M713049 (A.L.) and
587 2021M703092 (J. W.), the Ganghong Young Scholar Development Fund (R.D.Y.),
588 the Kobilka Institute of Innovative Drug Discovery at The Chinese University of Hong
589 Kong, Shenzhen (Y.D., R.D.Y.). The authors thank the Kobilka Cryo-Electron
590 Microscopy Center in the Chinese University of Hong Kong, Shenzhen for cryo-
591 electron microscopy analysis. The computational work was supported by the
592 Warshel Institute for Computational Biology (funding from Shenzhen City and
593 Longgang District) and the fund from Shenzhen-Hong Kong Cooperation Zone for
594 Technology and Innovation (HZQB-KCZYB-2020056).

595 **Author Contributions:**

596 A.L. performed cloning, protein expression and purification of the human GPR1
597 protein for complex formation, screening of cryo-EM grids, collection of cryo-EM data
598 and building of the structural model; Y.L. conducted mutagenesis analysis, functional
599 assays, structural comparison and figure preparation; G.C. assisted in structural
600 model building; W.L. and L.Z. performed MD simulation; J.W. and F.Y. provided
601 purified G proteins and Nano-BiT constructs used in this study; Y.D. and R.D.Y.
602 designed and supervised the research; Y.L. and R.D.Y. wrote the manuscript.

603 **Competing Interest Statement:**

604 The authors declare no competing interest.

605

606

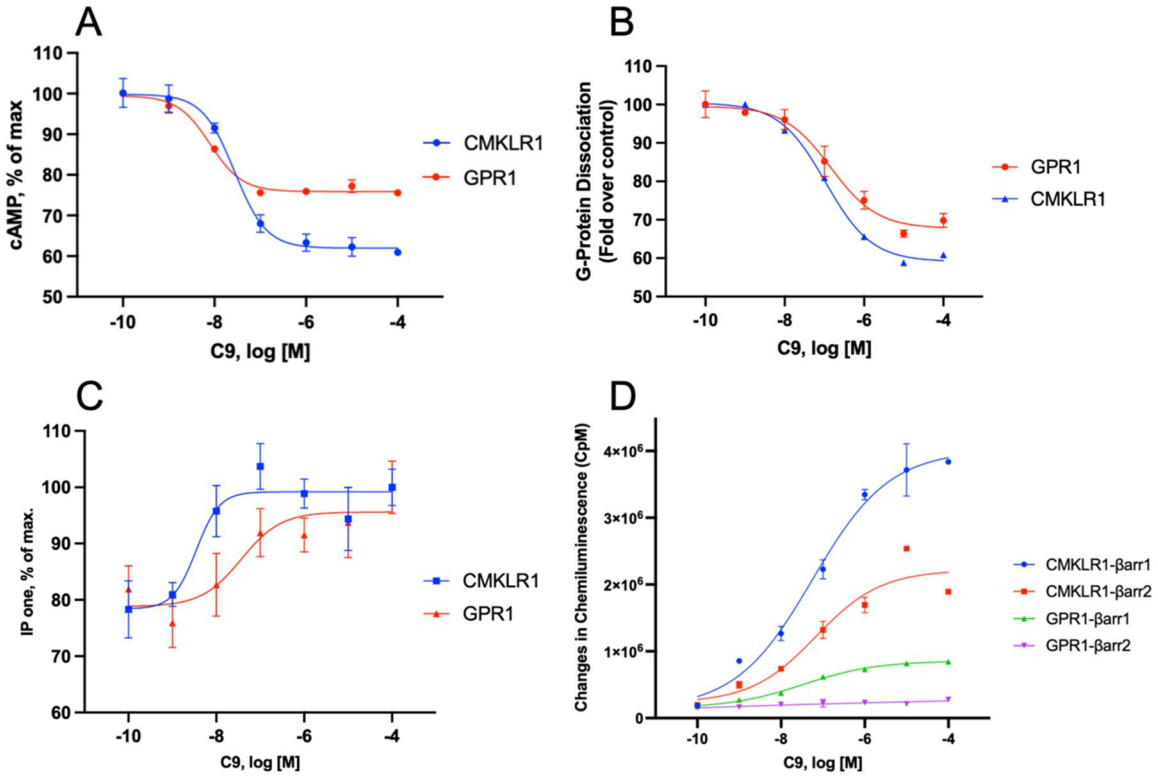

Figure 1. cAMP inhibition, G protein dissociation, IP one and β-arrestin responses of GPR1. (A) cAMP inhibition response of GPR1 and CMKLR1 stimulated by different concentrations of C9. **(B)** NanoBiT G protein dissociation response of GPR1 and CMKLR1 treated by different concentrations of C9. **(C)** Accumulation of IP-one upon treatment of different concentrations of C9 on GPR1 and CMKLR1. **(D)** NanoBiT β-arrestin recruitment of GPR1 and CMKLR1 upon stimulation of different concentration of C9. Data are shown as means ± SEM from three independent experiments.

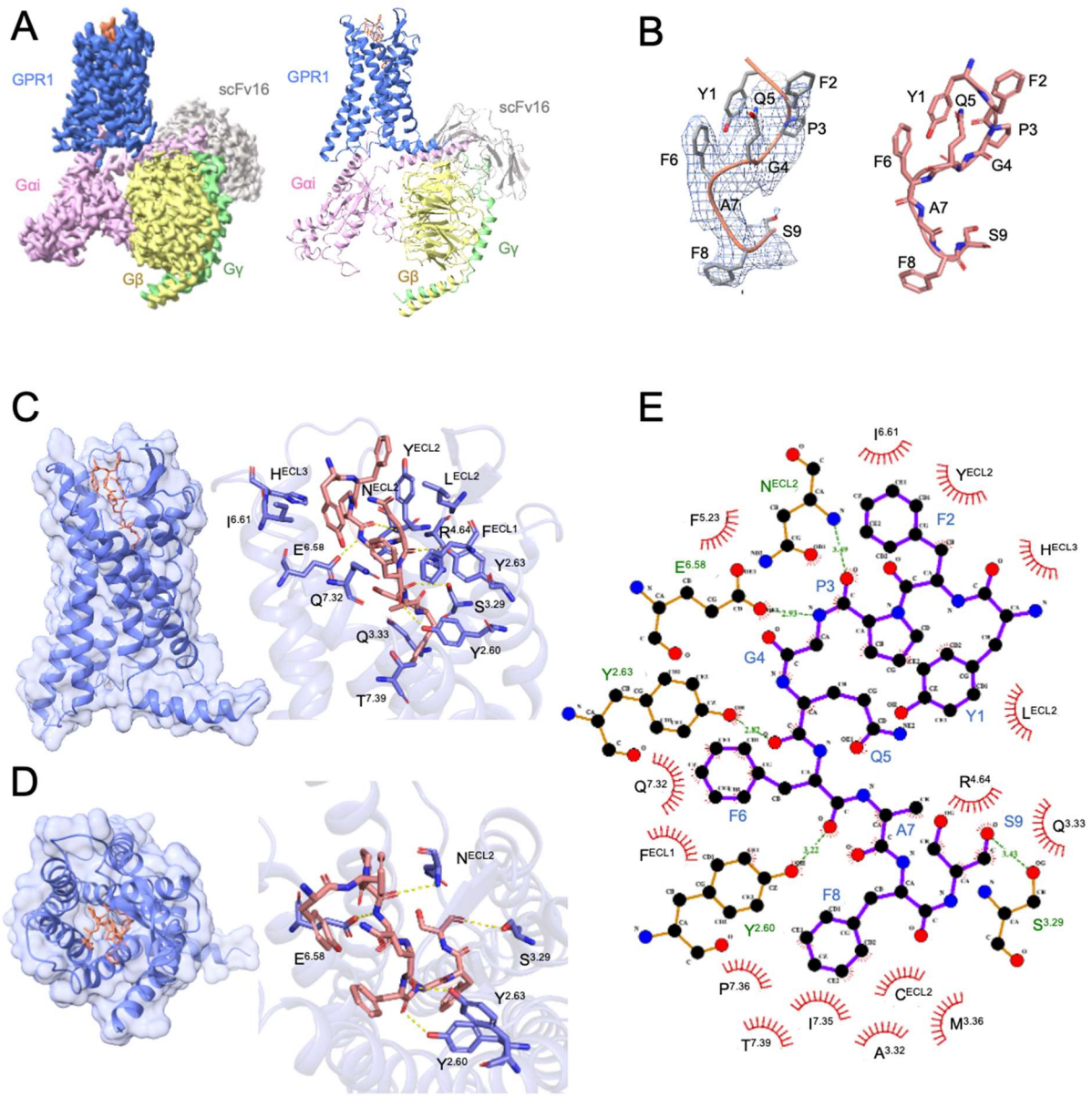

Figure 2. Overall structure and ligand binding pocket of C9-GPR1-Gi complex. **(A)** Cryo-EM density map (left) and the structural model (right) of the GPR1-Gi-scFv16 complex bound to C9. **(B)** Cryo-EM density map (left) and the peptide backbone (right) of C9. **(C)** Overall structure of GPR1-C9 complex from side view (left) and key interaction residues (right). In the overall structure, the receptor (marine blue) is shown in cartoon and surface representation. The C9 peptide is shown in sticks with carbon in salmon orange. The residues of GPR1 within 4 Å from the C9 peptide (salmon orange licorice and ribbon) are shown in marine blue licorice. The hydrogen bonds are displayed as dashed lines. **(D)** Extracellular view of the overall structure (left) and polar interactions (right) of the GPR1-C9 complex. The residue numbering of GPR1 follows the Ballesteros–Weinstein nomenclature. **(E)** Schematic representation of interactions between GPR1 and C9 analyzed by LigPlot+ program. The stick representations of GPR1 and C9 are shown as orange and purple sticks, respectively.

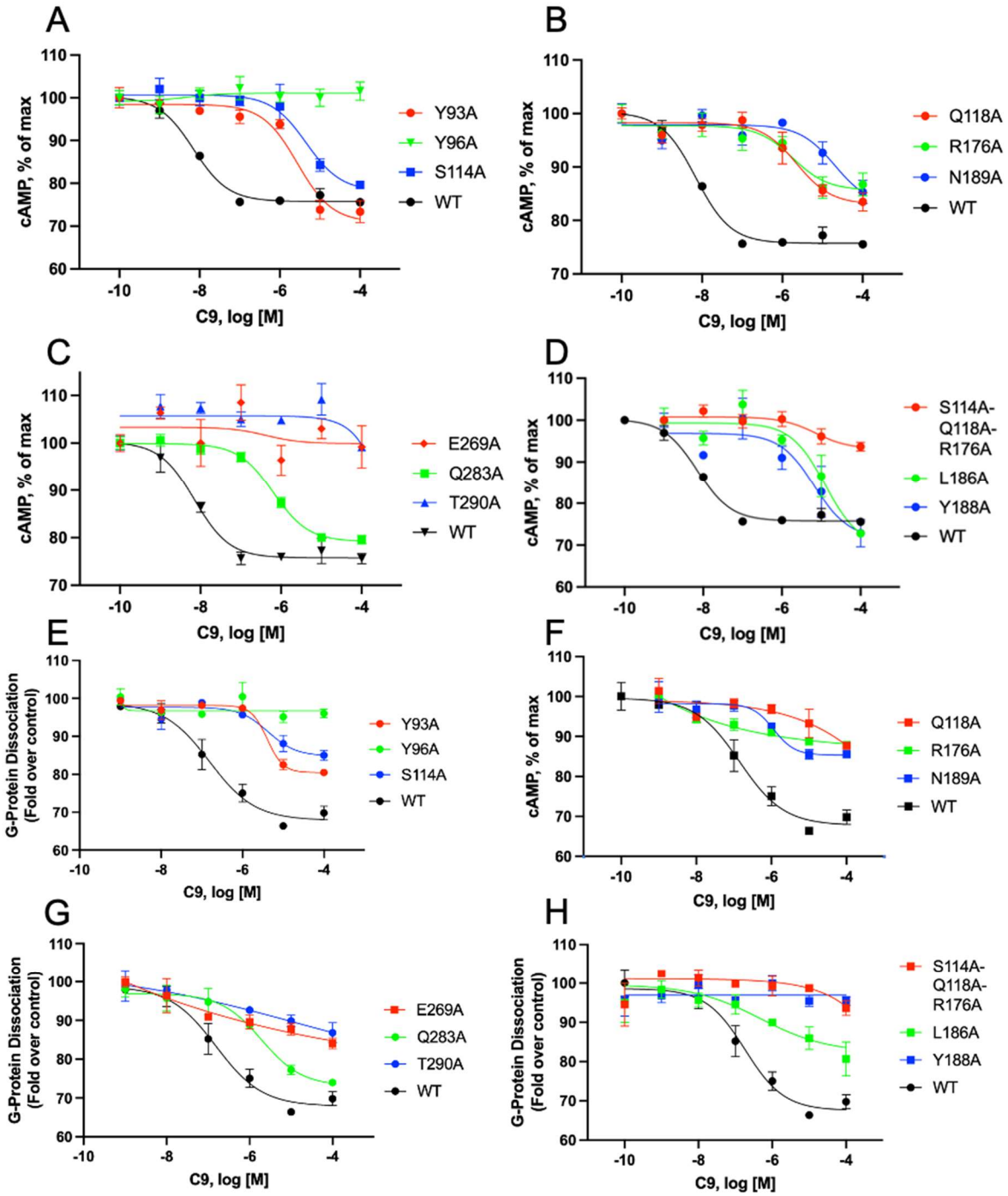

Figure 3. Structural mutants of C9-GPR1 binding pocket affect ligand-induced cAMP inhibition and G protein dissociation. (A - D) cAMP response in HeLa cells transfected to express WT or mutant GPR1. Different concentrations of C9 are applied. **(E - H)** G protein dissociation in HEK293T cells co-transfected to express WT or mutant GPR1, Gαi1-LgBiT, Gβ1, and SmBiT-Gγ2. Different concentrations of C9 are applied. All data shown are means ± SEM from three independent experiments.

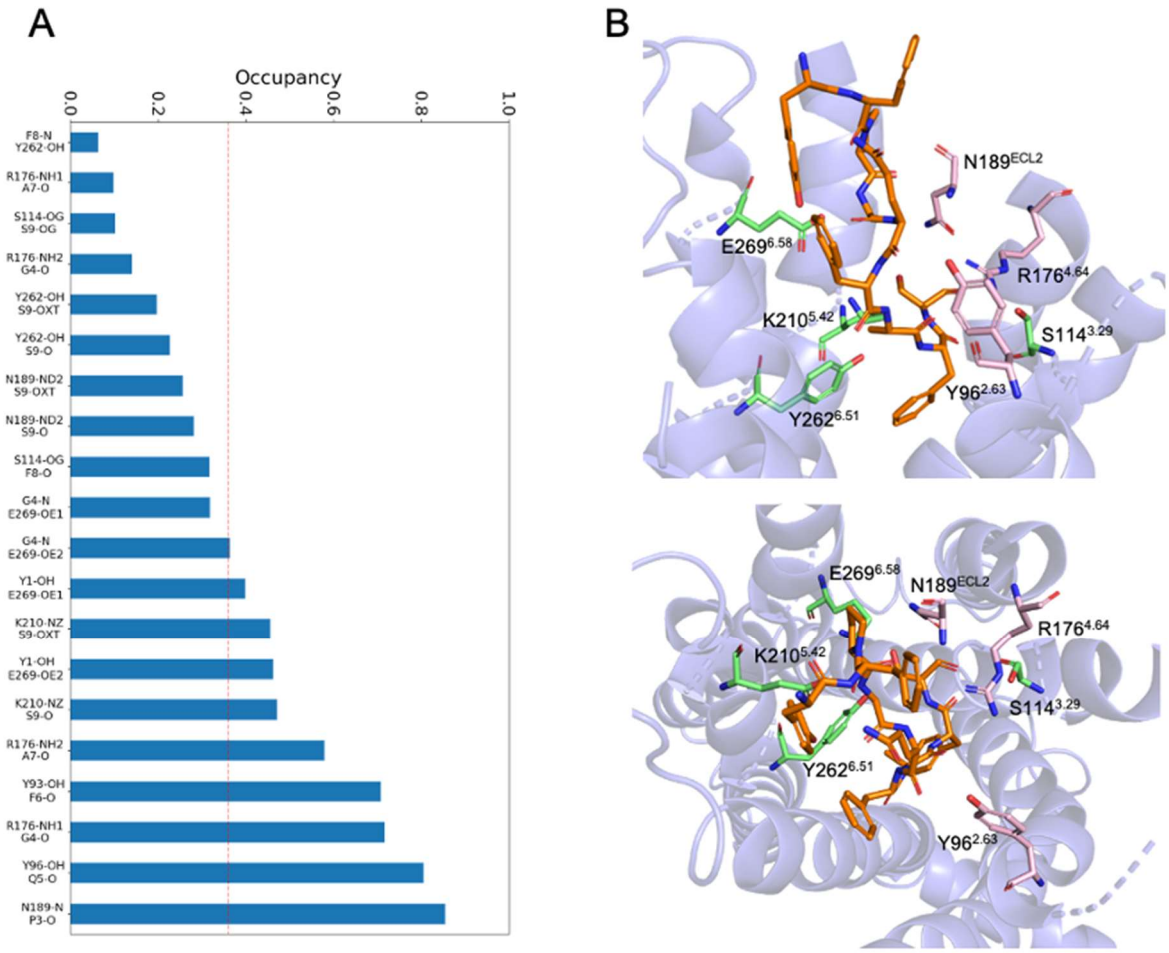

Figure 4. Thermodynamic stability analysis of the GPR1-C9 interface with µs-scale MD simulations. (A) The occupancy of all H-bonds between C9 and GPR1 observed in MD simulations. **(B)** Side view (upper panel) and top view (lower panel) of the distributions of functionally related residues around the C9 peptide.

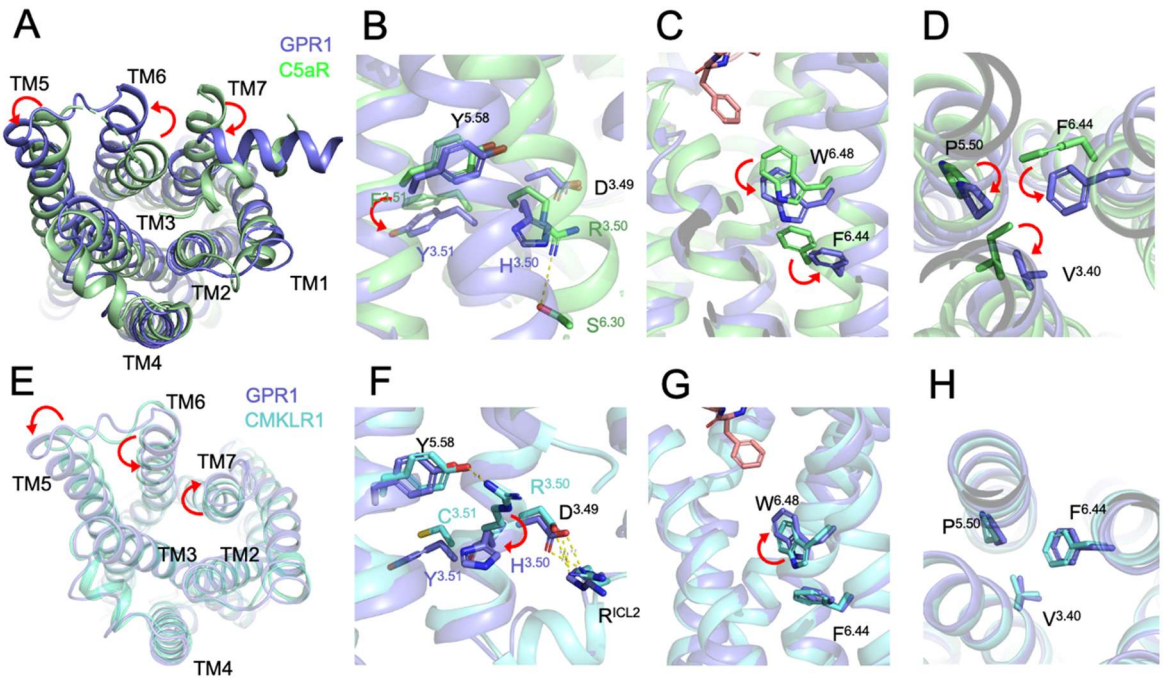

Figure 5. Comparison of GPCR structural motifs for G protein activation. (A) Intracellular view of the movement of GPR1 transmembrane helix 5, 6, and 7 (shown in marine blue) in comparison with inactive C5aR (PDB ID: 6C1R, shown in lime green). **(B)** Side close-up view of the $D^{3.49}$-$R^{3.50}$-$Y^{3.51}$ motif. A downward movement of $Y^{3.51}$ of GPR1 is highlighted by a red arrow. **(C)** Side close-up view of the "toggle switch", $W^{6.48}$ and $F^{6.44}$, an anti-clockwise rotation is highlighted for GPR1. **(D)** Rotamer conformational changes at the $P^{5.50}$-I/$V^{3.40}$-$F^{6.44}$ motif of GPR1 and C5aR, respectively. **(E)** Intracellular view of the movement of GPR1 transmembrane helix 5, 6, and 7 (shown in marine blue) in comparison with active CMKLR1 (PDB ID: 7YKD, shown in cyan). **(F)** Side close-up view of the $D^{3.49}$-$R^{3.50}$-$Y^{3.51}$ motif. A downward movement of $H^{3.50}$ of GPR1 is highlighted by a red arrow. **(G)** Side close-up view of the "toggle switch", $W^{6.48}$ and $F^{6.44}$, a clockwise rotation is highlighted for GPR1. **(H)** No significant conformational change at $P^{5.50}$-I/$V^{3.40}$-$F^{6.44}$ motif of GPR1 and CMKLR1, respectively.

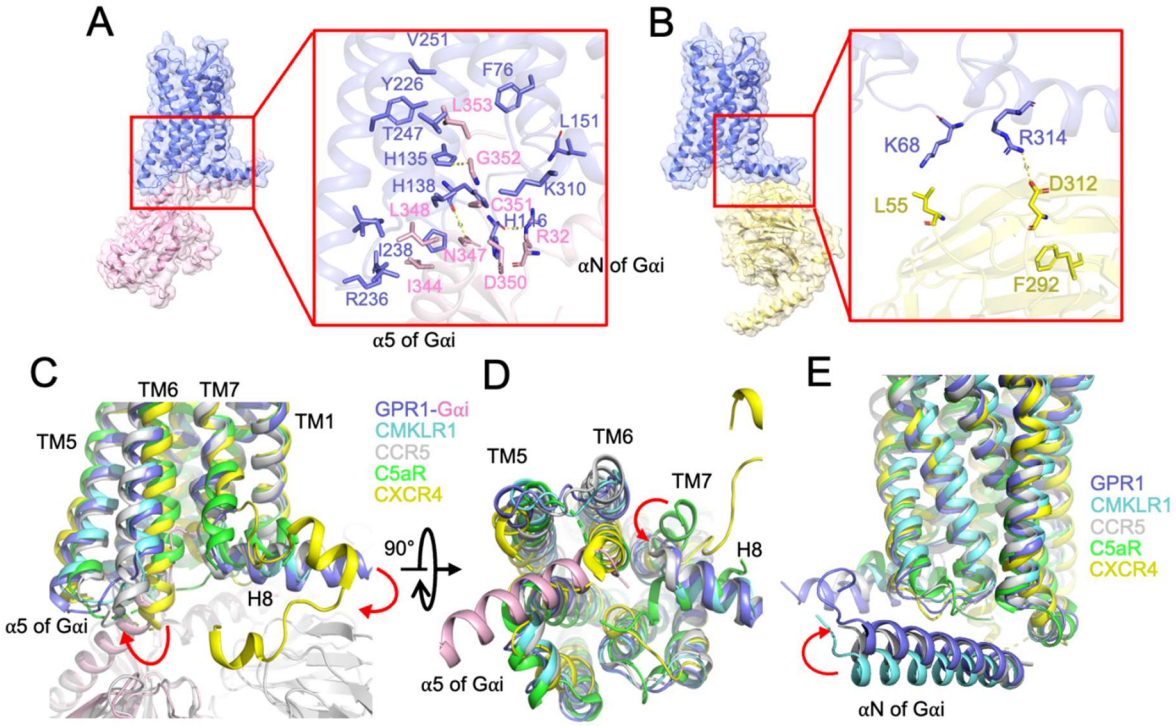

Figure 6. G protein interface of the C9-bound GPR1-Gi complex. (A) The interactions between the α5 helix of Gαi (pink) and GPR1 (marine blue) in the cavity at ICL3, TM5, TM6, and TM7 regions. **(B)** The interactions between Gβ subunit (yellow) and H8 of the receptor (marine blue). **(C)** Comparisons of the interactions between the α5 helix of Gαi and TM5, TM6, and ICL3 of several Gi-coupled receptors including GPR1 (marine blue), CMKLR1 (cyan, PDB ID: 7YKD), CCR5 (gray, PDB ID: 7F1R), C5aR (lime green, PDB ID: 6C1R) and CXCR4 (yellow, PDB ID: 3ODU). **(D)** 90°orientation of (C) for intracellular view showing the locations of ICL2, ICL1, and H8. **(E)** Same as (C) and (D) yet the interactions of the αN helix of Gαi with these receptors are compared.

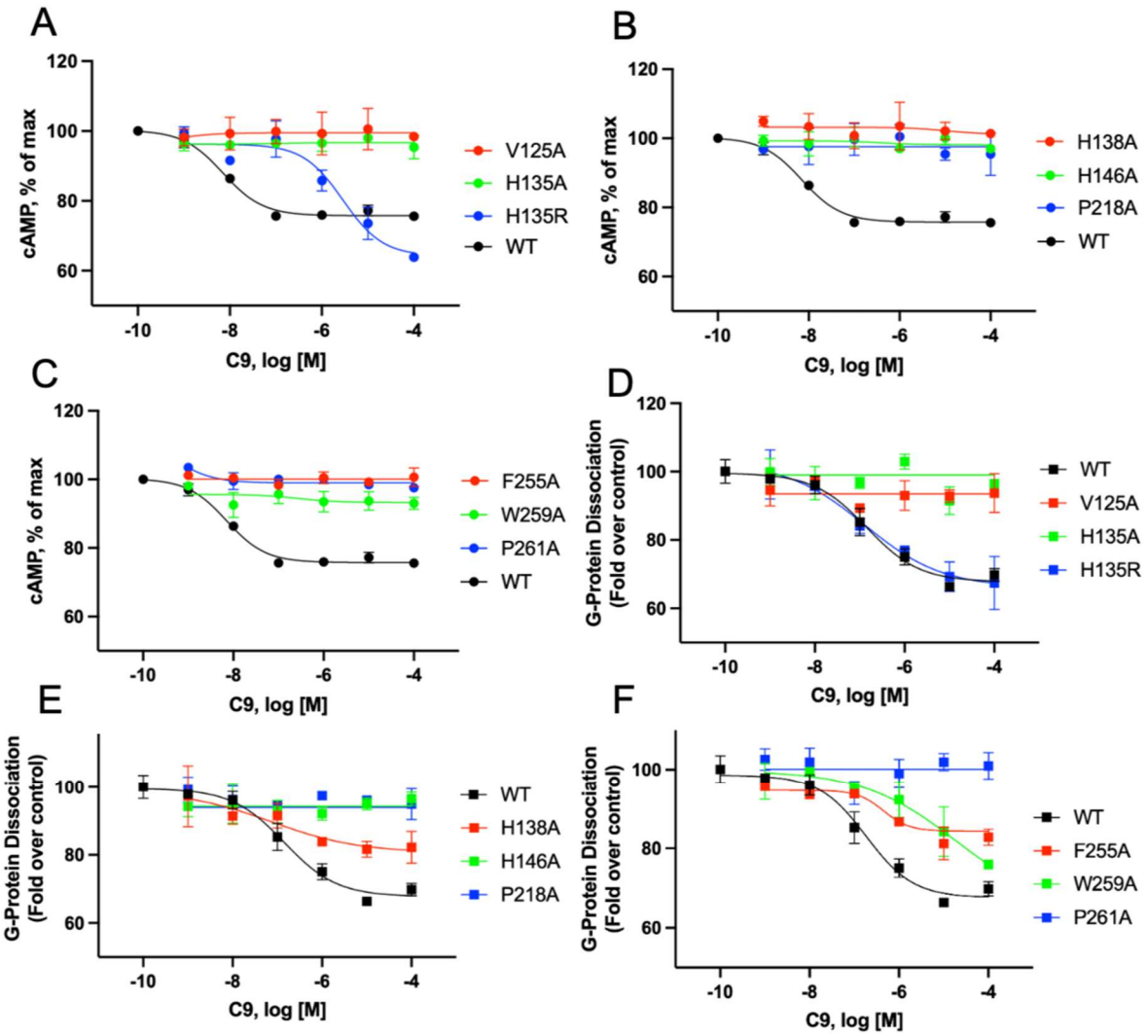

Figure 7. Point mutations at key residues for G protein activation affect cAMP inhibition and G protein dissociation. (A - C) cAMP response in HeLa cells transfected to express WT or mutant GPR1. Different concentrations of C9 are applied. **(D - F)** G protein dissociation in HEK293T cells co-transfected to express WT or mutant GPR1, Gαi1-LgBiT, Gβ1, and SmBiT-Gγ2. Different concentrations of C9 are applied. All data shown are means ± SEM from three independent experiments.

References:

Anandakrishnan, R., Aguilar, B., & Onufriev, A. V. (2012). H++ 3.0: automating pK prediction and the preparation of biomolecular structures for atomistic molecular modeling and simulations. *Nucleic Acids Res*, *40*(Web Server issue), W537-541. https://doi.org/10.1093/nar/gks375

Ballesteros, J. A., & Weinstein, H. (1995). Integrated methods for the construction of three-dimensional models and computational probing of structure-function relations in G protein-coupled receptors. In *Methods in neurosciences* (Vol. 25, pp. 366-428). Elsevier.

Barnea, G., Strapps, W., Herrada, G., Berman, Y., Ong, J., Kloss, B., Axel, R., & Lee, K. J. (2008). The genetic design of signaling cascades to record receptor activation. *Proc Natl Acad Sci U S A*, *105*(1), 64-69. https://doi.org/10.1073/pnas.0710487105

Bozaoglu, K., Bolton, K., McMillan, J., Zimmet, P., Jowett, J., Collier, G., Walder, K., & Segal, D. (2007). Chemerin is a novel adipokine associated with obesity and metabolic syndrome. *Endocrinology*, *148*(10), 4687-4694. https://doi.org/10.1210/en.2007-0175

Caulfield, M., Munroe, P., Pembroke, J., Samani, N., Dominiczak, A., Brown, M., Benjamin, N., Webster, J., Ratcliffe, P., O'Shea, S., Papp, J., Taylor, E., Dobson, R., Knight, J., Newhouse, S., Hooper, J., Lee, W., Brain, N., Clayton, D., . . . Study, M. R. C. B. G. o. H. (2003). Genome-wide mapping of human loci for essential hypertension. *Lancet*, *361*(9375), 2118-2123. https://doi.org/10.1016/S0140-6736(03)13722-1

Chen, G., Wang, X., Liao, Q., Ge, Y., Jiao, H., Chen, Q., Liu, Y., Lyu, W., Zhu, L., van Zundert, G. C. P., Robertson, M. J., Skiniotis, G., Du, Y., Hu, H., & Ye, R. D. (2022). Structural basis for recognition of N-formyl peptides as pathogen-associated molecular patterns. *Nat Commun*, *13*(1), 5232. https://doi.org/10.1038/s41467-022-32822-y

Chen, T., Xiong, M., Zong, X., Ge, Y., Zhang, H., Wang, M., Won Han, G., Yi, C., Ma, L., Ye, R. D., Xu, Y., Zhao, Q., & Wu, B. (2020). Structural basis of ligand binding modes at the human formyl peptide receptor 2. *Nat Commun*, *11*(1), 1208. https://doi.org/10.1038/s41467-020-15009-1

Chun, E., Thompson, A. A., Liu, W., Roth, C. B., Griffith, M. T., Katritch, V., Kunken, J., Xu, F., Cherezov, V., Hanson, M. A., & Stevens, R. C. (2012). Fusion partner toolchest for the stabilization and crystallization of G protein-coupled receptors. *Structure*, *20*(6), 967-976. https://doi.org/10.1016/j.str.2012.04.010

De Henau, O., Degroot, G. N., Imbault, V., Robert, V., De Poorter, C., McHeik, S., Gales, C., Parmentier, M., & Springael, J. Y. (2016). Signaling Properties of Chemerin Receptors CMKLR1, GPR1 and CCRL2. *PLoS One*, *11*(10), e0164179. https://doi.org/10.1371/journal.pone.0164179

Degroot, G. N., Lepage, V., Parmentier, M., & Springael, J. Y. (2022). The Atypical Chemerin Receptor GPR1 Displays Different Modes of Interaction with beta-Arrestins in Humans and Mice with Important Consequences on Subcellular Localization and Trafficking. *Cells*, *11*(6). https://doi.org/10.3390/cells11061037

Ernst, M. C., & Sinal, C. J. (2010). Chemerin: at the crossroads of inflammation and obesity. *Trends Endocrinol Metab*, *21*(11), 660-667. https://doi.org/10.1016/j.tem.2010.08.001

Fischer, T. F., Czerniak, A. S., Weiß, T., Schoeder, C. T., Wolf, P., Seitz, O., Meiler, J., & Beck-Sickinger, A. G. (2021). Ligand-binding and -scavenging of the chemerin receptor GPR1. *Cellular and Molecular Life Sciences*, *78*(17-18), 6265-6281. https://doi.org/10.1007/s00018-021-03894-8

Goralski, K. B., Jackson, A. E., McKeown, B. T., & Sinal, C. J. (2019). More Than an Adipokine: The Complex Roles of Chemerin Signaling in Cancer. *Int J Mol Sci*, *20*(19). https://doi.org/10.3390/ijms20194778

Goralski, K. B., McCarthy, T. C., Hanniman, E. A., Zabel, B. A., Butcher, E. C., Parlee, S. D., Muruganandan, S., & Sinal, C. J. (2007). Chemerin, a novel adipokine that regulates

803 adipogenesis and adipocyte metabolism. *J Biol Chem*, *282*(38), 28175-28188.
804 https://doi.org/10.1074/jbc.M700793200
805 Helfer, G., & Wu, Q. F. (2018). Chemerin: a multifaceted adipokine involved in metabolic
806 disorders. *J Endocrinol*, *238*(2), R79-R94. https://doi.org/10.1530/JOE-18-0174
807 Herova, M., Schmid, M., Gemperle, C., & Hersberger, M. (2015). ChemR23, the receptor for
808 chemerin and resolvin E1, is expressed and functional on M1 but not on M2
809 macrophages. *J Immunol*, *194*(5), 2330-2337.
810 https://doi.org/10.4049/jimmunol.1402166
811 Huang, J., Rauscher, S., Nawrocki, G., Ran, T., Feig, M., de Groot, B. L., Grubmuller, H., &
812 MacKerell, A. D., Jr. (2017). CHARMM36m: an improved force field for folded and
813 intrinsically disordered proteins. *Nat Methods*, *14*(1), 71-73.
814 https://doi.org/10.1038/nmeth.4067
815 Inoue, A., Raimondi, F., Kadji, F. M. N., Singh, G., Kishi, T., Uwamizu, A., Ono, Y., Shinjo,
816 Y., Ishida, S., Arang, N., Kawakami, K., Gutkind, J. S., Aoki, J., & Russell, R. B.
817 (2019). Illuminating G-Protein-Coupling Selectivity of GPCRs. *Cell*, *177*(7), 1933-
818 1947 e1925. https://doi.org/10.1016/j.cell.2019.04.044
819 Karagiannis, G. S., Weile, J., Bader, G. D., & Minta, J. (2013). Integrative pathway dissection
820 of molecular mechanisms of moxLDL-induced vascular smooth muscle phenotype
821 transformation. *BMC Cardiovasc Disord*, *13*, 4. https://doi.org/10.1186/1471-2261-13-
822 4
823 Kennedy, A. J., & Davenport, A. P. (2018a). International Union of Basic and Clinical
824 Pharmacology CIII: Chemerin Receptors CMKLR1 (Chemerin1) and GPR1
825 (Chemerin2) Nomenclature, Pharmacology, and Function. *Pharmacol Rev*, *70*(1),
826 174-196. https://doi.org/10.1124/pr.116.013177
827 Kennedy, A. J., & Davenport, A. P. (2018b). International Union of Basic and Clinical
828 Pharmacology CIII: Chemerin Receptors CMKLR1 (Chemerin(1)) and GPR1
829 (Chemerin(2)) Nomenclature, Pharmacology, and Function. *Pharmacol Rev*, *70*(1),
830 174-196. https://doi.org/10.1124/pr.116.013177
831 Kennedy, A. J., Yang, P., Read, C., Kuc, R. E., Yang, L., Taylor, E. J., Taylor, C. W.,
832 Maguire, J. J., & Davenport, A. P. (2016). Chemerin Elicits Potent Constrictor Actions
833 via Chemokine-Like Receptor 1 (CMKLR1), not G-Protein-Coupled Receptor 1
834 (GPR1), in Human and Rat Vasculature. *J Am Heart Assoc*, *5*(10).
835 https://doi.org/10.1161/JAHA.116.004421
836 Kleist, A. B., Getschman, A. E., Ziarek, J. J., Nevins, A. M., Gauthier, P. A., Chevigne, A.,
837 Szpakowska, M., & Volkman, B. F. (2016). New paradigms in chemokine receptor
838 signal transduction: Moving beyond the two-site model. *Biochem Pharmacol*, *114*,
839 53-68. https://doi.org/10.1016/j.bcp.2016.04.007
840 Lee, E., Taussig, R., & Gilman, A. G. (1992). The G226A mutant of Gs alpha highlights the
841 requirement for dissociation of G protein subunits. *J Biol Chem*, *267*(2), 1212-1218.
842 https://www.ncbi.nlm.nih.gov/pubmed/1730644
843 Lehrke, M., Becker, A., Greif, M., Stark, R., Laubender, R. P., von Ziegler, F., Lebherz, C.,
844 Tittus, J., Reiser, M., Becker, C., Goke, B., Leber, A. W., Parhofer, K. G., & Broedl,
845 U. C. (2009). Chemerin is associated with markers of inflammation and components
846 of the metabolic syndrome but does not predict coronary atherosclerosis. *Eur J*
847 *Endocrinol*, *161*(2), 339-344. https://doi.org/10.1530/EJE-09-0380
848 Maeda, S., Koehl, A., Matile, H., Hu, H., Hilger, D., Schertler, G. F. X., Manglik, A., Skiniotis,
849 G., Dawson, R. J. P., & Kobilka, B. K. (2018). Development of an antibody fragment
850 that stabilizes GPCR/G-protein complexes. *Nat Commun*, *9*(1), 3712.
851 https://doi.org/10.1038/s41467-018-06002-w
852 Marchese, A., Docherty, J. M., Nguyen, T., Heiber, M., Cheng, R., Heng, H. H., Tsui, L. C.,
853 Shi, X., George, S. R., & O'Dowd, B. F. (1994). Cloning of human genes encoding
854 novel G protein-coupled receptors. *Genomics*, *23*(3), 609-618.
855 https://doi.org/10.1006/geno.1994.1549
856 Meder, W., Wendland, M., Busmann, A., Kutzleb, C., Spodsberg, N., John, H., Richter, R.,
857 Schleuder, D., Meyer, M., & Forssmann, W. G. (2003). Characterization of human

858 circulating TIG2 as a ligand for the orphan receptor ChemR23. *FEBS Lett*, *555*(3),
859 495-499. https://doi.org/10.1016/s0014-5793(03)01312-7
860 Neves, K. B., Nguyen Dinh Cat, A., Alves-Lopes, R., Harvey, K. Y., Costa, R. M. D., Lobato,
861 N. S., Montezano, A. C., Oliveira, A. M., Touyz, R. M., & Tostes, R. C. (2018).
862 Chemerin receptor blockade improves vascular function in diabetic obese mice via
863 redox-sensitive and Akt-dependent pathways. *Am J Physiol Heart Circ Physiol*,
864 *315*(6), H1851-H1860. https://doi.org/10.1152/ajpheart.00285.2018
865 Posner, B. A., Mixon, M. B., Wall, M. A., Sprang, S. R., & Gilman, A. G. (1998). The A326S
866 mutant of Gialpha1 as an approximation of the receptor-bound state. *J Biol Chem*,
867 *273*(34), 21752-21758. https://doi.org/10.1074/jbc.273.34.21752
868 Rourke, J. L., Dranse, H. J., & Sinal, C. J. (2015). CMKLR1 and GPR1 mediate chemerin
869 signaling through the RhoA/ROCK pathway. *Mol Cell Endocrinol*, *417*, 36-51.
870 https://doi.org/10.1016/j.mce.2015.09.002
871 Rourke, J. L., Muruganandan, S., Dranse, H. J., McMullen, N. M., & Sinal, C. J. (2014). Gpr1
872 is an active chemerin receptor influencing glucose homeostasis in obese mice. *J*
873 *Endocrinol*, *222*(2), 201-215. https://doi.org/10.1530/JOE-14-0069
874 Samson, M., Edinger, A. L., Stordeur, P., Rucker, J., Verhasselt, V., Sharron, M., Govaerts,
875 C., Mollereau, C., Vassart, G., Doms, R. W., & Parmentier, M. (1998). ChemR23, a
876 putative chemoattractant receptor, is expressed in monocyte-derived dendritic cells
877 and macrophages and is a coreceptor for SIV and some primary HIV-1 strains. *Eur J*
878 *Immunol*, *28*(5), 1689-1700. https://doi.org/10.1002/(SICI)1521-
879 4141(199805)28:05<1689::AID-IMMU1689>3.0.CO;2-I
880 Schulz, R., Korkut-Demirbas, M., Venturino, A., Colombo, G., & Siegert, S. (2022). Chimeric
881 GPCRs mimic distinct signaling pathways and modulate microglia responses. *Nat*
882 *Commun*, *13*(1), 4728. https://doi.org/10.1038/s41467-022-32390-1
883 Shimizu, N., Tanaka, A., Oue, A., Mori, T., Ohtsuki, T., Apichartpiyakul, C., Uchiumi, H.,
884 Nojima, Y., & Hoshino, H. (2009). Broad usage spectrum of G protein-coupled
885 receptors as coreceptors by primary isolates of HIV. *AIDS*, *23*(7), 761-769.
886 https://doi.org/10.1097/QAD.0b013e328326cc0d
887 Surgand, J. S., Rodrigo, J., Kellenberger, E., & Rognan, D. (2006). A chemogenomic
888 analysis of the transmembrane binding cavity of human G-protein-coupled receptors.
889 *Proteins*, *62*(2), 509-538. https://doi.org/10.1002/prot.20768
890 Tokizawa, S., Shimizu, N., Hui-Yu, L., Deyu, F., Haraguchi, Y., Oite, T., & Hoshino, H.
891 (2000). Infection of mesangial cells with HIV and SIV: identification of GPR1 as a
892 coreceptor. *Kidney Int*, *58*(2), 607-617. https://doi.org/10.1046/j.1523-
893 1755.2000.00207.x
894 Wang, J., Chen, G., Liao, Q., Lyu, W., Liu, A., Zhu, L., Du, Y., & Ye, R. D. (2023). Cryo-EM
895 structure of the human chemerin receptor 1-Gi protein complex bound to the C-
896 terminal nonapeptide of chemerin. *Proc Natl Acad Sci U S A*, *120*(11), e2214324120.
897 https://doi.org/10.1073/pnas.2214324120
898 Weis, W. I., & Kobilka, B. K. (2018). The Molecular Basis of G Protein-Coupled Receptor
899 Activation. *Annu Rev Biochem*, *87*, 897-919. https://doi.org/10.1146/annurev-
900 biochem-060614-033910
901 Wittamer, V., Franssen, J. D., Vulcano, M., Mirjolet, J. F., Le Poul, E., Migeotte, I., Brezillon,
902 S., Tyldesley, R., Blanpain, C., Detheux, M., Mantovani, A., Sozzani, S., Vassart, G.,
903 Parmentier, M., & Communi, D. (2003). Specific recruitment of antigen-presenting
904 cells by chemerin, a novel processed ligand from human inflammatory fluids. *J Exp*
905 *Med*, *198*(7), 977-985. https://doi.org/10.1084/jem.20030382
906 Wittamer, V., Gregoire, F., Robberecht, P., Vassart, G., Communi, D., & Parmentier, M.
907 (2004). The C-terminal nonapeptide of mature chemerin activates the chemerin
908 receptor with low nanomolar potency. *J Biol Chem*, *279*(11), 9956-9962.
909 https://doi.org/10.1074/jbc.M313016200
910 Zabel, B. A., Allen, S. J., Kulig, P., Allen, J. A., Cichy, J., Handel, T. M., & Butcher, E. C.
911 (2005). Chemerin activation by serine proteases of the coagulation, fibrinolytic, and

inflammatory cascades. *J Biol Chem*, *280*(41), 34661-34666. https://doi.org/10.1074/jbc.M504868200

Zabel, B. A., Nakae, S., Zuniga, L., Kim, J. Y., Ohyama, T., Alt, C., Pan, J., Suto, H., Soler, D., Allen, S. J., Handel, T. M., Song, C. H., Galli, S. J., & Butcher, E. C. (2008). Mast cell-expressed orphan receptor CCRL2 binds chemerin and is required for optimal induction of IgE-mediated passive cutaneous anaphylaxis. *J Exp Med*, *205*(10), 2207-2220. https://doi.org/10.1084/jem.20080300

Zabel, B. A., Silverio, A. M., & Butcher, E. C. (2005). Chemokine-like receptor 1 expression and chemerin-directed chemotaxis distinguish plasmacytoid from myeloid dendritic cells in human blood. *J Immunol*, *174*(1), 244-251. https://doi.org/10.4049/jimmunol.174.1.244

Zheng, C., Chen, D., Zhang, Y., Bai, Y., Huang, S., Zheng, D., Liang, W., She, S., Peng, X., Wang, P., Mo, X., Song, Q., Lv, P., Huang, J., Ye, R. D., & Wang, Y. (2018). FAM19A1 is a new ligand for GPR1 that modulates neural stem-cell proliferation and differentiation. *FASEB J*, fj201800020RRR. https://doi.org/10.1096/fj.201800020RRR

Zhou, Q., Yang, D., Wu, M., Guo, Y., Guo, W., Zhong, L., Cai, X., Dai, A., Jang, W., Shakhnovich, E. I., Liu, Z. J., Stevens, R. C., Lambert, N. A., Babu, M. M., Wang, M. W., & Zhao, S. (2019). Common activation mechanism of class A GPCRs. *Elife*, *8*. https://doi.org/10.7554/eLife.50279

Zhu, Y., Lin, X., Zong, X., Han, S., Wang, M., Su, Y., Ma, L., Chu, X., Yi, C., Zhao, Q., & Wu, B. (2022). Structural basis of FPR2 in recognition of Abeta42 and neuroprotection by humanin. *Nat Commun*, *13*(1), 1775. https://doi.org/10.1038/s41467-022-29361-x

Zhuang, Y., Liu, H., Edward Zhou, X., Kumar Verma, R., de Waal, P. W., Jang, W., Xu, T. H., Wang, L., Meng, X., Zhao, G., Kang, Y., Melcher, K., Fan, H., Lambert, N. A., Eric Xu, H., & Zhang, C. (2020). Structure of formylpeptide receptor 2-Gi complex reveals insights into ligand recognition and signaling. *Nat Commun*, *11*(1), 885. https://doi.org/10.1038/s41467-020-14728-9

Zhuang, Y., Wang, L., Guo, J., Sun, D., Wang, Y., Liu, W., Xu, H. E., & Zhang, C. (2022). Molecular recognition of formylpeptides and diverse agonists by the formylpeptide receptors FPR1 and FPR2. *Nat Commun*, *13*(1), 1054. https://doi.org/10.1038/s41467-022-28586-0